Superhydrophobic Polypropylene Surfaces Prepared with TiO_2 Nanoparticles Functionalized by Dendritic Polymers

Cintia B. Contreras,[1,2]* Francisco N. Figueroa,[1,2] Daniel E. Weibel,[3] Miriam C. Strumia [1,2]

[1]Facultad de Ciencias Químicas, Departamento de Química Orgánica, Laboratorio de Materiales Poliméricos (LAMAP), Universidad Nacional de Córdoba, Córdoba, Argentina
[2]CONICET, Instituto de Investigación y Desarrollo de Ingeniería de Procesos y Química Aplicada (IPQA), Haya de la Torre y Medina Allende, Ciudad Universitaria (X5000HUA), Córdoba, Argentina
[3]Laboratório de Fotoquímica e Superfícies, Departamento de Físico-Química, Instituto de Química, UFRGS, Av. Bento Gonçalves 9500, Bairro Agronomia CEP: 91501-970, CP 15003, Porto Alegre, RS, Brasil
Correspondence to: M. C. Strumia (E-mail: mcs@fcq.unc.edu.ar)

Received 27 March 2018; accepted 2 June 2018; published online 00 Month 2018
DOI: 10.1002/pola.29086

ABSTRACT: Hybrid inorganic–organic nanomaterials have received increasing interest due to the possibility of implementing different functions and characteristics within a single material. Their functionalities are a consequence of the synergy of the properties of distinct building blocks and are related to their varied natures and spatial locations. In this work, we present the development of superhydrophobic properties on polypropylene (PP) surfaces using hybrid nanomateriales from TiO_2 nanoparticles (NPs) and dendronized polymers. The dendron acryl Behera's amine was successfully grafted on the TiO_2 NP surfaces by Surface-Initiated Atom Transfer Radical Polymerization (SI-ATRP) and a core-brush material was obtained. Finally, PP substrates were coated with NP hybrids to produce superhydrophobic surfaces with water contact angles of over 158 degrees. Controlling the organic silane concentration on the TiO_2 NPs allowed the dendronized process to be driven and thereby permitted the selection of specific wettability properties on PP substrate surfaces with high water adhesion or self-cleaning conditions. This dendronized effect with consequent steric congestion of the polymeric brushes on the NPs changed their behaviors from Wenzel to the Cassie Baxter state. © 2017 Wiley Periodicals, Inc. J. Polym. Sci., Part A: Polym. Chem. **2017**, *00*, 000–000

KEYWORDS: dendronized polymers; hybrid materials; SI-ATRP; superhydrophobic surfaces

INTRODUCTION One of chemist's goals is to create complex materials with well-defined structures and functionalities as occurs in nature. The advances made in modern synthetic tools and methodologies have allowed a number of artificial materials and structures to be constructed that imitate natural products. One exciting achievement in materials and polymer chemistry in recent decades is the capability to create large synthetic nanostructures with well-defined shapes and atomic structures in a rational and efficient manner.[1,2] One example is the bio-inspired non-wettable surface which has many practical applications, including the separation of oil/water dispersions, self-cleaning, drag reduction, anti-fogging, anti-bacteria, anti-fouling, anti-icing, and corrosion resistance, among others.[3–7] Those achievements were inspired by the impressive wettability properties of natural surfaces, such as lotus leaves, rice leaves, red rose petals, the Chinese watermelon surface, butterfly wings, water striders' legs, and the skins of fish and shark, with many artificial surfaces with superhydrophobic properties having now been fabricated. However, there have been very few reports about new combined synthetic methodologies for the fabrication of a specific nanostructuration.[4,8–11]

The surface free energy and the geometrical morphology of the surfaces are the most important parameters which affect the wettability of the material.[12] In this regard, a low surface free energy and enhanced surface roughness with hierarchical micro- and nano-sized structures are essential for preparing superhydrophobic surfaces.[13–16] Two important models for describing the wettability behavior of a rough surface were presented by Wenzel[17] and by Cassie and Baxter,[18] which are commonly used to explain the effect of roughness on the apparent contact angle of a liquid droplet on a solid surface. In many cases, the fabrication of artificial hierarchical micro-nano

**Present address:* Cintia B. Contreras, Instituto de Nanosistemas, Universidad Nacional de San Martín. Av. 25 de Mayo 1021. B1650. San Martín, Buenos Aires, Argentina

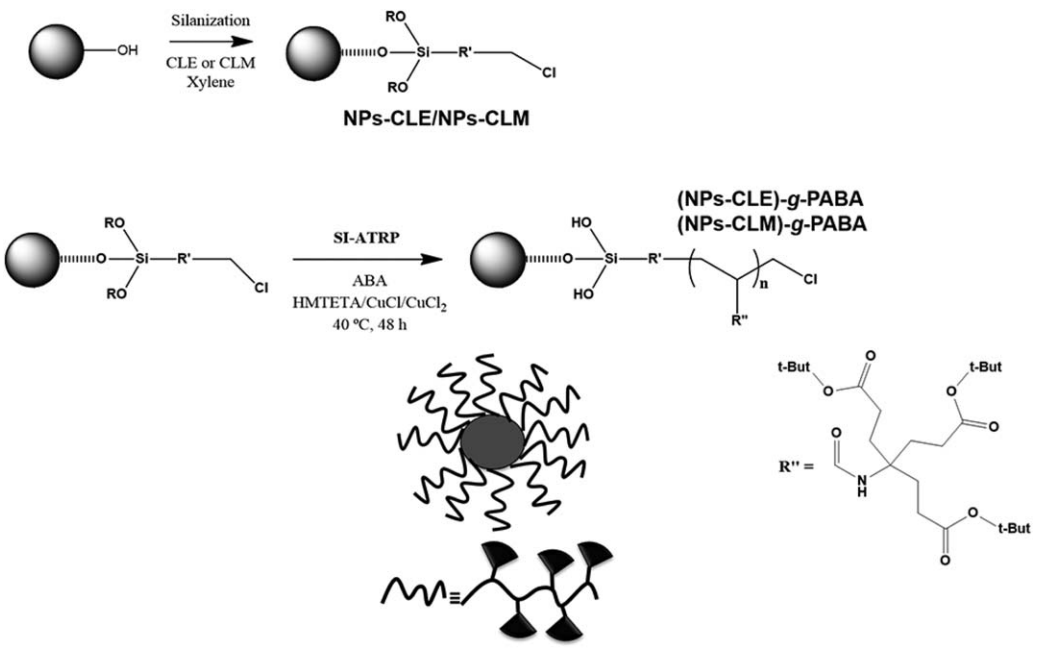

SCHEME 1 Surface modification on TiO_2 NPs by SI-ATRP.

structures is obtained by selecting a specific surface's modification processes in order to control both the chemical composition and the surface morphology.[19–23]

The fabrication of artificial superhydrophobic surfaces can be achieved using several methods, such as lithography, template-based techniques, plasma treatments, self-assembly, chemical deposition, layer-by-layer (LBL) deposition, colloidal assembly, phase separation, and electrospinning.[24–29] Another synthetic way is by chemical modification using conveniently functionalized building blocks. In this approach, dendronized nanostructures are used, which consist of hyperbranched building blocks combined with other species, such as inorganic nanoparticles, linear polymers, and polymeric surfaces. This represents a promising approach using multifunctional materials for a wide range of potential applications, from materials science to molecular biology.[30,31] The main interest in these types of multifunctional materials is based on their possibility to exhibit new unexpected behaviors, rather than on the sum of individual components.[32]

A large number of dendronized polymers based on different types of polymer backbones, and dendrons have been developed by three main synthetic approaches: "graft-to," "graft-from," and "macromonomer."[32–34] It has been clearly demonstrated that the size, rigidity, and functionality of dendronized polymers can be altered by controlling their molecular compositions and architectures.[35–39] Our research group has described the use of Newkome-type dendrons as modification agents, in particular di-tert-butyl-4-amino-4-[2-(tert-butoxycarbonyl)ethyl]heptanedioate, which is commercially known as aminotriester.[37,40–43]

This article presents a new synthetic methodology of nanostructuration of Polypropylene (PP) surfaces, with the aim of obtaining superhydrophobic properties. Previously, dendronized TiO_2 nanoparticles (NPs) were prepared by grafting, after which, they were used as building blocks to modify the PP surfaces by dip-coating. Enhanced properties of micro- and nanostructures were produced by our method, including a high static contact angle, good adhesion of the coating to the PP, and most importantly, the concentration of dendronized polymers could be tuned to obtain superhydrophobicity with or without self-cleaning properties.

RESULTS AND DISCUSSION

Surface Modification of TiO_2 Nanoparticles

First of all, the dendritic monomer [Acryl Behera's Amine (ABA)] was prepared according to a procedure described by Cuggino et al.[44]

Surface modification of the TiO_2 NPs was performed in two steps as shown in Scheme 1. In the first step of the synthesis, the surface of TiO_2 NPs was functionalized by a reaction with an organic silane agent [(3-chloropropyl) triethoxysilane, CLE, or (3-chloropropyl) trimethoxysilane, CLM], which was subsequently used in a second step, as an SI-ATRP initiator for grafting polymerization. After this, type core-brush NPs of TiO_2 were obtained with brushes of poly(ABA) (PABA).

Table 1 summarizes all the reactions performed and the products obtained. The two series obtained were (NPs-CLM^a)-*g*-PABA and (NPs-CLE^a)-*g*-PABA. The ratio "*a*" denotes the organic silane concentration used (organic silane/xylene ratio). If *a* increases, the amount of organic silane bonded to the surface of the NPs rises, implying more initiating sites per particle and as a consequence of the ATRP mechanism, the number of polymeric chains per particle also increases.

Figure 1 shows the DRIFT-FTIR spectra of unmodified TiO_2 NPs and the hybrid material produced. Strong absorption

TABLE 1 Evaluated conditions for the production of hybrid materials obtained from the ABA grafting (6×10^{-5} mol/mg NPs) on the surface of TiO_2 nanoparticles at 40 °C for 48 h

Serie	Silane Agent	[Silane/ Xylene] (v/v)	Hybrid Material
(NPs-CLM)-*g*-PABA	CLM	1/99	No products
		5/95	(NPs-CLM$^{5/95}$)-*g*-PABA
		10/90	(NPs-CLM$^{10/90}$)-*g*-PABA
(NPs-CLE)-*g*-PABA	CLE	1/99	No products
		5/95	(NPs-CLE$^{5/95}$)-*g*-PABA
		10/90	(NPs-CLE$^{10/90}$)-*g*-PABA

bands at around 3450 and 1640 cm^{-1} were observed in the unmodified TiO_2, due to the —OH stretching vibrations and H—O—H bending vibrations on the surface of the nanoparticles, respectively. Furthermore, a strong absorption band from 450 to 950 cm^{-1} was observed due to the O—Ti—O stretching vibration. Upon graft polymerization of the TiO_2 nanoparticles, other intense bands appeared. The bands from PABA were: 1720 cm^{-1} stretching C═O (ester), 1650 cm^{-1} C═O (amide), and 850 cm^{-1} bending C—H (*t*-butyl group), with this later band being overlapped with the O—Ti—O stretching from the TiO_2. As no differences in the behavior or yields were observed by the use of both organic silane agents, the rest of experiments were carried out with NPs-CLE.

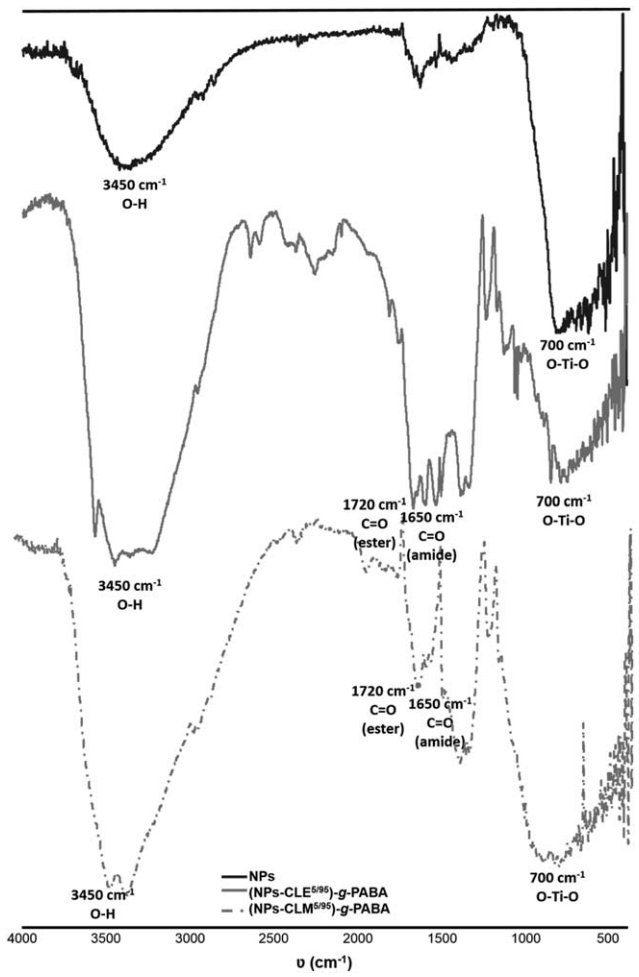

FIGURE 1 DRIFT-FTIR spectra of unmodified TiO_2 NPs and the hybrid material produced.

The morphology of the nanoparticles was observed by TEM. The TEM images of bare TiO_2 and silanizated TiO_2 are shown in Figure 2, where the bare TiO_2 exhibited an average external diameter of about 30 ± 1 nm. In addition, unmodified TiO_2 NPs were characterized by a non-uniform globular form and were found to be agglomerated. The silanized TiO_2 NPs also revealed agglomeration of the NPs and same average size than the bare NPs.

TEM images from the hybrid material are presented in Figure 3. After grafting with PABA, the diameters of the NPs became a little larger, with some core/brush structures where the organic polymeric layer could be observed. The width of the layer formed by these brushes was around 2.5 ± 0.5 nm and 5.0 ± 0.5 nm, for (NPs-CLE$^{5/95}$)-*g*-PABA [Fig. 3(ii)] and (NPs-CLE$^{10/90}$)-*g*-PABA [Fig. 3(ii)], respectively. Visualization by TEM of the layer around the NPs together with the ATR-FTIR data confirmed that the PABA polymer chains were linked to TiO_2 NPs. In Figure 3, it is possible to observe an apparent layer coating the NPs in some cases. However due to the overlapping of several NPs, it is not possible to conclude from the TEM images that the NPs are complete or partially coated by polymeric brushes. However, TEM image of the functionalized NPs which performed the ATRP procedure without the monomer (Fig. 3-i) did not present any core/shell structures.

The thermal properties of unmodified TiO_2 NPs and TiO_2 NPs grafted with PABA [(NPs-CLE)-*g*-PABA] were evaluated using TGA, as shown in Figure 4. The weight loss of unmodified TiO_2 was less than 3% when heated from room temperature to 600 °C, which was mostly due to the evaporation of absorbed water. For the grafted TiO_2 NPs, (NPs-CLE)-*g*-PABA, two weight losses were observed. The first weight loss was observed after heating to 240 °C, which until 100 °C was due to water being strongly absorbed,[45] after which it was mostly attributable to *t*-butyl groups of the PABA units, as previously reported.[46] The second weight loss took place between 240 and 500 °C, from a process corresponding to the progressive thermal decomposition of the remaining organic content. This occurred in several closely related but undistinguished stages, thereby making the assignation of the fragments impossible. From 500 °C, all thermograms remained constant. Consequently, the organic content of each system as well as the organic loading achieved at each synthetic step was calculated by taking into consideration the weight loss occurring between 100 and 500 °C, with a weight loss of 15.63% and 21.68% being found for (NPs-CLE$^{5/95}$)-*g*-PABA and (NPs-CLE$^{10/90}$)-*g*-PABA, respectively. These weight loss values for the composite particles depended on the initiator concentration of the controlled polymerization.

The percentage of modification (p) of TiO_2 NPs by PABA, was calculated from eq 1 using the TGA data.

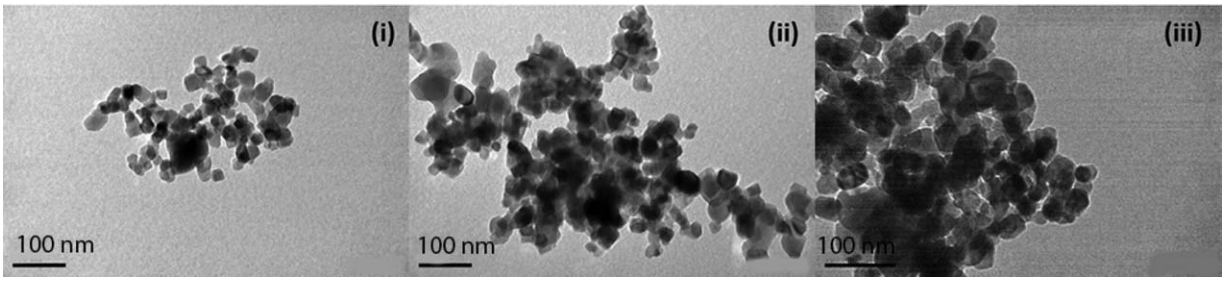

FIGURE 2 TEM images of unmodified TiO_2 nanoparticles (i), silanized TiO_2 nanoparticles: NPs-CLE$^{5/95}$ (ii), and NPs-CLM$^{5/95}$ (iii).

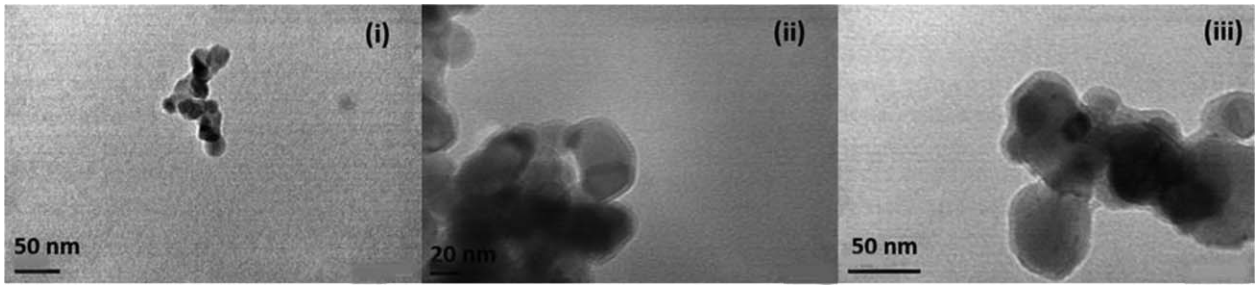

FIGURE 3 TEM images of: functionalized NPs which performed the ATRP procedure without the monomer (i), and hybrid materials (NPs-CLE$^{5/95}$)-*g*-PABA (ii) and (NPs-CLE$^{10/90}$)-*g*-PABA (iii).

$$p(\%) = \text{weight loss}_{(\text{NPs}-\text{CLE}-g-\text{PABA})} - \text{weight loss}_{\text{NPs}} \quad (1)$$

The *p* (%) was found to be 13.17% and 19.22% for the systems (NPs-CLE$^{5/95}$)-*g*-PABA and (NPs-CLE$^{10/90}$)-*g*-PABA, respectively. As observed by other techniques, these results for composite particles depend on the initiator concentration due to the controlled polymerization."

Finally, the gyration radius (*Rg*) was calculated from SAXS measurements, as shown in Figure 5. By assuming that the particles are spherical (a simplified assumption) and using the Guinier approximation,[47] the *Rg* were obtained from the plot of ln [*I*(*q*)] versus q^2 at q_{min}*$Rg < 1.5$ and the radius of the particles (*r*) was derived from eq 2.

$$Rg = \sqrt{\frac{3}{5}}r \quad (2)$$

Unmodified nanoparticles had an *Rg* of around 10 nm and (NPs-CLE)-*g*-PABA nanoparticles presented smaller *Rg*, of 8 and 9 nm for (NPs-CLE$^{5/95}$)-*g*-PABA and (NPs-CLE$^{10/90}$)-*g*-PABA, respectively. The *Rg* for the grafted TiO_2 NPs, (NPs-CLE)-*g*-PABA was smaller than that unmodified particles, due to their agglomeration. In addition, for the values of *r* calculated of 106.7 and 135.0 nm for (NPs-CLE$^{5/95}$)-*g*-PABA and (NPs-CLE$^{10/90}$)-*g*-PABA, respectively, we were able to observe that the polymer brushes depended on the initiator concentration.

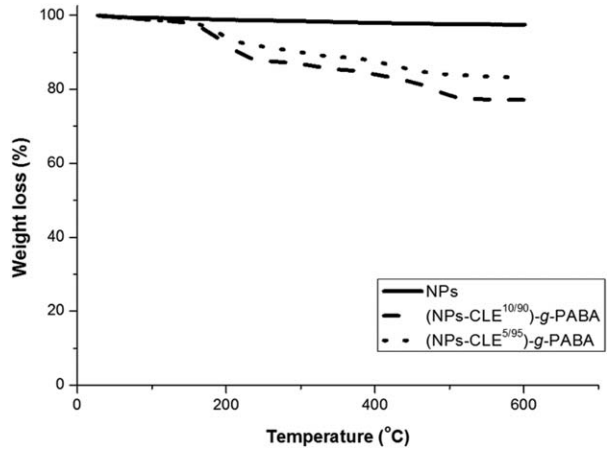

FIGURE 4 TGA data of unmodified TiO_2 nanoparticles and TiO_2 nanoparticles grafted with PABAs: (NPs-CLE$^{5/95}$)-*g*-PABA and (NPs-CLE$^{10/90}$)-*g*-PABA.

Construction of Superhydrophobic Surfaces

Superhydrophobic surfaces were obtained using a simple one-step dip-nano composite coating method on PP sticks.[25] Scheme 2 shows the methodology used for obtaining the surface modification of the PP sticks using grafted TiO_2 NPs to obtain (NPs-CLE)-*g*-PABA.

Modified PP surfaces were studied using ATR-FTIR (symbol of Attenuated Total Reflectance Fourier Transform Infrared) spectroscopy, and the results demonstrated a successful surface modification of the PP sticks (Fig. 6). In particular, the 1720 cm^{-1} stretching C═O (ester) band confirmed the presence of (NPs-CLE)-*g*-PABA on the modified surfaces of the sticks.

Surface morphology was investigated by SEM and profilometry. Figure 7 presents SEM images of the PP sticks modified with (NPs-CLE$^{5/95}$)-*g*-PABA and (NPs-CLE$^{10/90}$)-*g*-PABA. Both

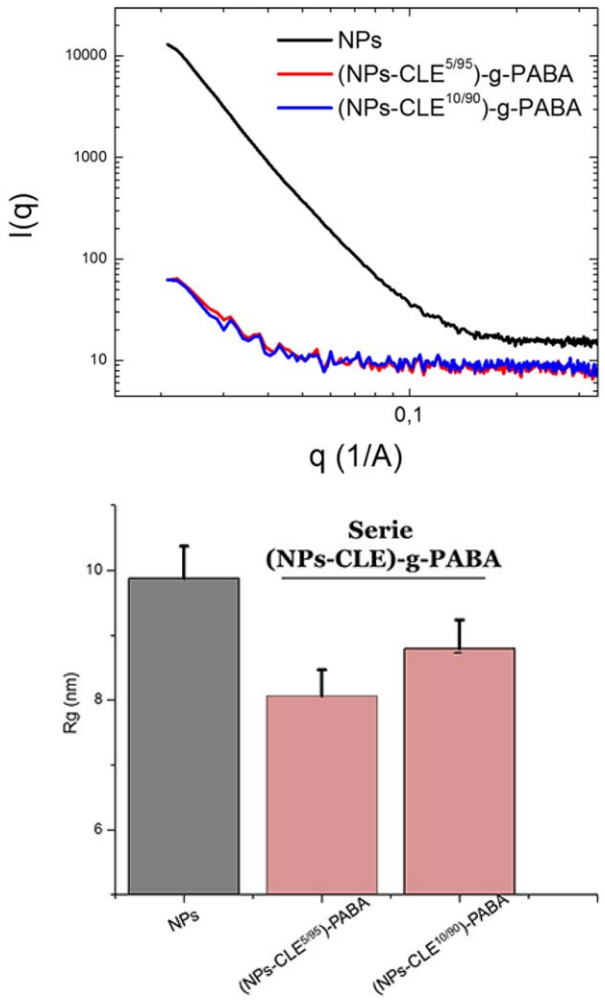

FIGURE 5 SAXS spectra and *Rg* obtained by the Guinier approximation from unmodified nanoparticles and (NPs-CLE)-*g*-PABA series. [Color figure can be viewed at wileyonlinelibrary.com]

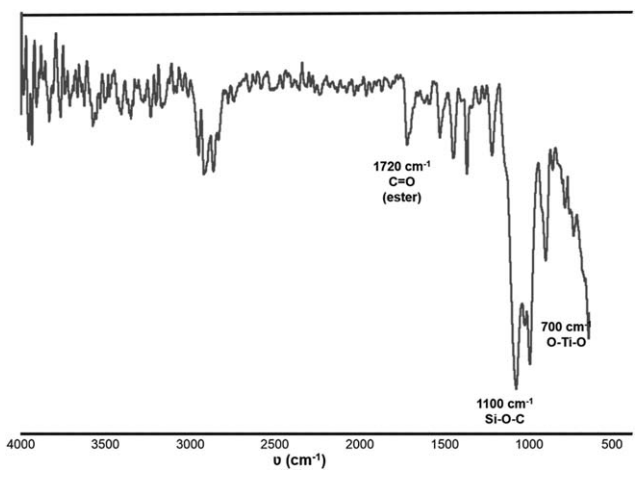

FIGURE 6 ATR-FTIR from PP stick modified with (NPs-CLE$^{10/90}$)-*g*-PABA nanoparticles.

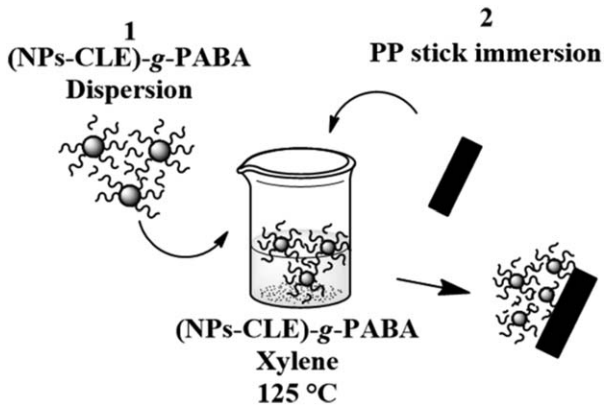

SCHEME 2 Schematic representation of the surface modification method of PP sticks by dip-coating with (NPs-CLE)-*g*-PABA nanoparticles.

modified surfaces presented rough heterogeneous ones with hierarchical micro- and nano-structure, although we did not observe significant differences in the topography or roughness of the surfaces under study. The PP (NPs-CLE$^{10/90}$)-*g*-PABA images may indicate a better coating of the surface.

Figure 8 presents profilometer images of each PP stick modified with (NPs-CLE$^{5/95}$)-*g*-PABA (left) and (NPs-CLE$^{10/90}$)-*g*-PABA (right). The RMS roughness increased from (0.25 ± 0.05) μm for unmodified PP to (1.0 ± 0.3) μm and (1.2 ± 0.3) μm for (NPs-CLE$^{10/90}$)-*g*-PABA and (NPs-CLE$^{5/95}$)-*g*-PABA, respectively. However, the roughness of PP modified surfaces were similar, but by comparison of the two profilometer images (top and bottom) for each sample we observed a better distribution and covering of the PP surface for a higher PABA concentration. In addition, a similar behavior was observed by SEM, as a consequence of the higher number of grafted chains on the surface, with only a small difference in height noted for (NPs-CLE$^{10/90}$)-*g*-PABA.

Finally, the wettability of the prepared surfaces was investigated by static water contact angle (WCA) measurements, and the results are shown in Table 2 and Figure 9. Unmodified PP showed a WCA of about 110 degrees, with superhydrophobic coatings being obtained from both modified PP substrates. The WCAs increased from 110 degrees for unmodified PP to 158 ± 7 and 162 ± 5 degrees for PP sticks modified with (NPs-CLE$^{5/95}$)-*g*-PABA and (NPs-CLE$^{10/90}$)-*g*-PABA, respectively. The PP stick modified with (NPs-CLE$^{5/95}$)-*g*-PABA presented a contact angle hysteresis (CAH) of 46 ± 5 degrees, while the PP stick modified with (NPs-CLE$^{10/90}$)-*g*-PABA revealed a CAH of 7.8 ± 0.7 degrees. Therefore, a small NPs-CLE$^{5/95}$ concentration produced an increase in the contact area liquid/solid and exhibited a Wenzel state. On the other hand, the higher NPs-CLE$^{10/90}$ gave a better surface coating with a small liquid/solid contact area, which produced the lowest hysteresis and showed a behavior corresponding to a Cassie Bexter state.

Profilometry measurements showed that the RMS of the PP substrates did not change appreciably between the (NPs-CLE$^{5/95}$)-g-PABA and (NPs-CLE$^{10/90}$)-g-PABA coatings,

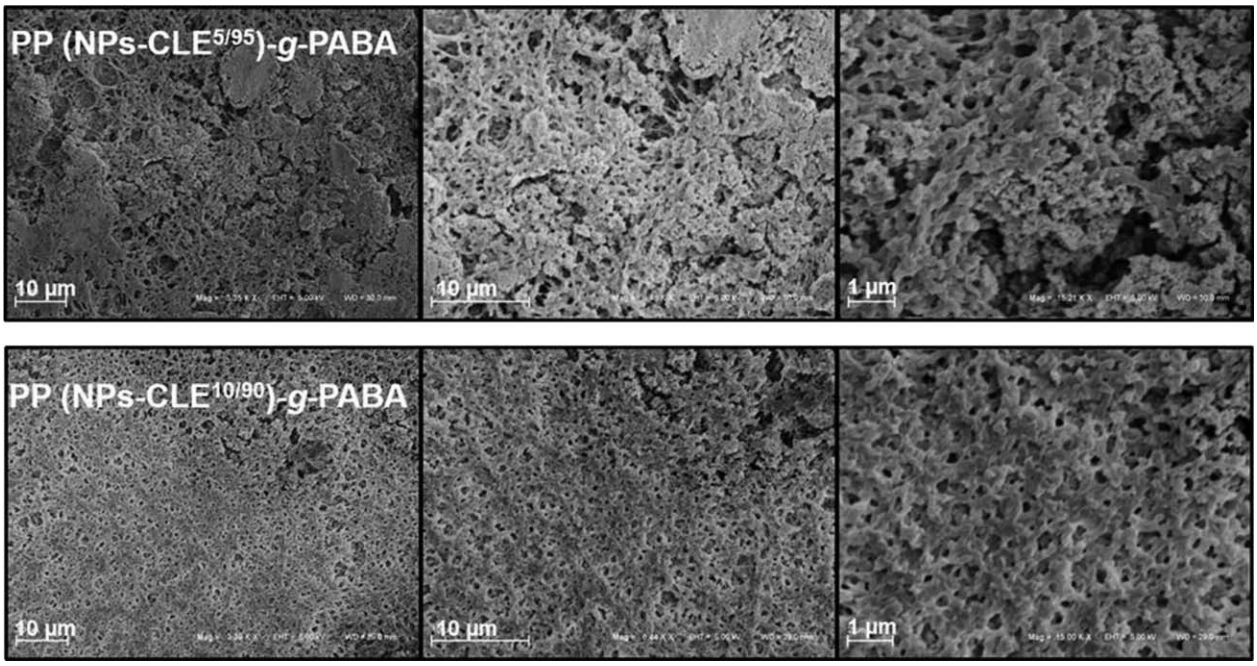

FIGURE 7 SEM images from PP stick modified with (NPs-CLE$^{5/95}$)-*g*-PABA and (NPs-CLE$^{10/90}$)-*g*-PABA.

$1.2 \pm 0.3\ \mu$m and $1.0 \pm 0.3\ \mu$m, respectively. In contrast, the very simple but high surface sensitive technique of WCA showed that the PP substrates coated with (NPs-CLE$^{10/90}$)-g-PABA produced a very efficient superhydrophobic coating due to the PP substrate self-cleaning properties. When (NPs-CLE$^{5/95}$)-g-PABA was used for the coating, the PP surfaces lost their low hysteresis, indicating partially coated TiO_2 NPs. Therefore, by regulating the silane concentration in the TiO_2 NPs functionalization, it is possible to control the grafted dendronized polymer and the superhydrophobic wettability properties of the prepared PP surfaces.

The coating adhesion to the PP stick was evaluated by a simple test using a 3M® tape. Figure 10 shows three optical microscope images obtained for each sample, corresponding to the PP stick before the test (left), PP stick after the test (middle) and tape after the test (right). In this test, we compared the adhesion properties with the superhydrophobic surfaces reported in our previous report,[25] in which the nanocomposite coatings on the PP stick samples were prepared by dipping them in xylene solvent containing titanium dioxide nanoparticles functionalized with trimethoxypropyl silane, TMPSi (serie a) and by also dipping them in a mixture

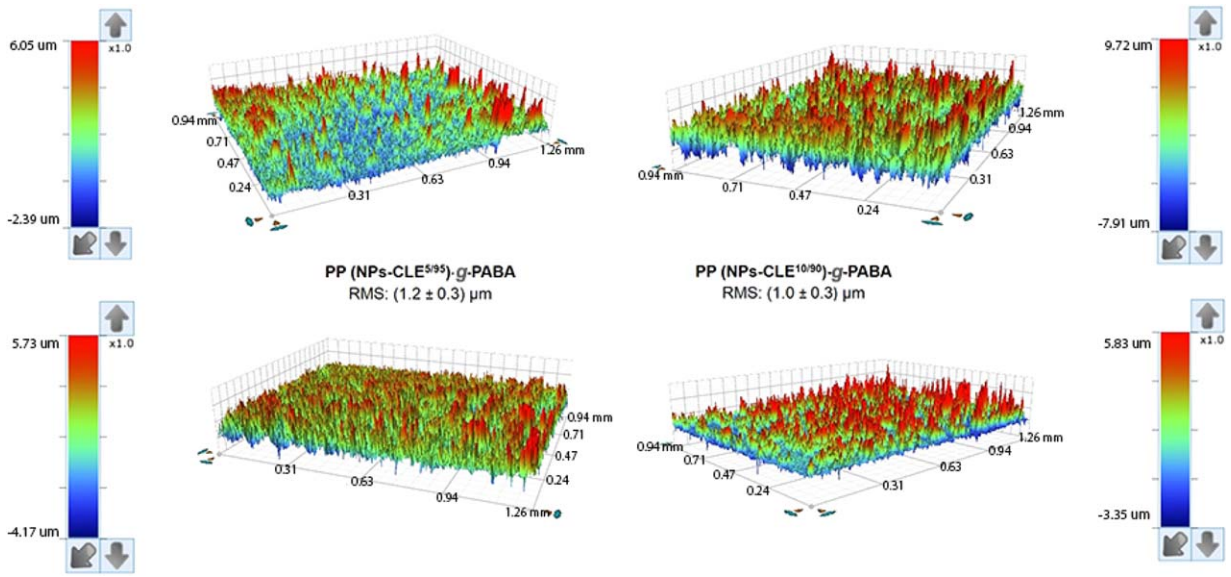

FIGURE 8 Profilometer images from PP stick modified with (NPs-CLE$^{5/95}$)-*g*-PABA (left) and (NPs-CLE$^{10/90}$)-*g*-PABA (right). [Color figure can be viewed at wileyonlinelibrary.com]

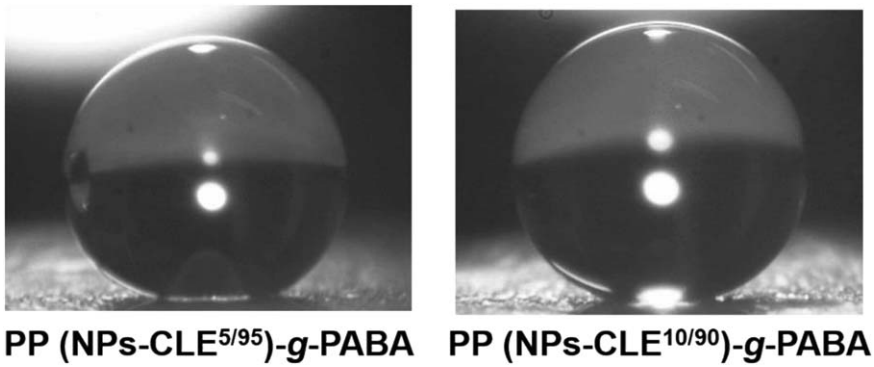

FIGURE 9 WCA from PP stick modified with (NPs-CLE$^{5/95}$)-*g*-PABA and (NPs-CLE$^{10/90}$)-*g*-PABA.

of functionalized NPs and dissolved PP pellets (serie b). The samples $\mathrm{NPs-PP}^{a}_{10/90}$, $\mathrm{NPs-PP}^{b}_{10/90}$ were chosen, were superscripts a and b represent series a or b, respectively; and 10/90 is the TMPSi concentration used. For both samples, tape images show the amount of coating removed after the test in white. While, in the case of the PP stick modified with (NPs-CLE$^{5/95}$)-*g*-PABA and (NPs-CLE$^{10/90}$)-*g*-PABA, the tape images reveal the amount of coating removed after the test in black. These results showed a poor adhesion between the coating and the PP stick in $\mathrm{NPs-PP}^{a}_{10/90}$, as in the tape

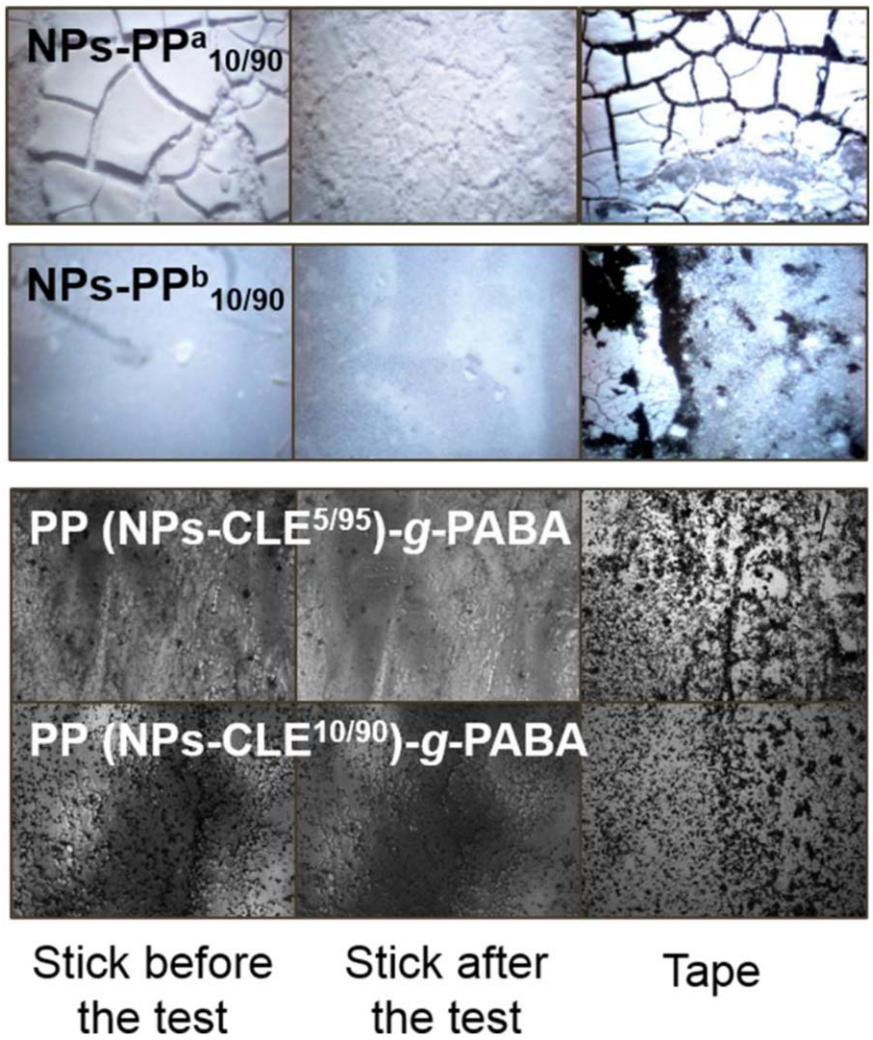

FIGURE 10 Optical microscopy images of the adhesion test. For each sample, stick before the test (left), stick after the test (middle), tape after the test (right). [Color figure can be viewed at wileyonlinelibrary.com]

TABLE 2 Static (WCA) and dynamic (CAH) water contact angle of PP films dip-coated with (NPs-CLE$^{5/95}$)-*g*-PABA and (NPs-CLE$^{10/90}$)-*g*-PABA

Surface	WCA (Mean ± SD)°	CAH (Mean ± SD)°
PP	110 ± 3	–
PP (NPs-CLE$^{5/95}$)-*g*-PABA	158 ± 7	46 ± 5
PP (NPs-CLE$^{10/90}$)-*g*-PABA	162 ± 6	7.8 ± 0.7

image an important amount of coating removed from the PP stick was observed. In contrast, in the case of NPs − PP$^{b}_{10/90}$, sample adhesion properties were improved with PP pellets being present during the dipping. This was due to the PP pellets being compatible agent. Although adhesion properties were improved by the PP pellets presence, they were still weak. On the other hand, for the (NPs-CLE$^{5/95}$)-*g*-PABA and (NPs-CLE$^{10/90}$)-*g*-PABA samples the tape images revealed a minimal amount of coating removed, so the adhesion properties were the best in this case. In addition, images of the PP stick showed its morphology was not changed after the test, and this advantage can be attributed to a covalent bond of the hydrophobic polymer and NPs surfaces.

DISCUSSION

The superhydrophobic properties were obtained for PP substrates modified with dendronized TiO_2 NPs. By *in situ* grafting, polymerization using SI-ATRP, TiO_2 NPs CLE$^{5/95}$-*g*-PABA and CLE$^{10/90}$-*g*-PABA was produced, with the grafting polymerization of (NPs-CLE$^{5/95}$)-*g*-PABA and (NPs-CLE$^{10/90}$)-*g*-PABA being confirmed by the ATR-FTIR, TGA, TEM and SAXS data. Next, by simple dip coating of the PP substrates in grafted TiO_2 NPs solutions, super-repellent surfaces were prepared. The presence of the dendronized TiO_2 NPs on the PP substrates was confirmed by ATR-FTIR producing a high increase in the RMS and WCA, compared with pure PP. The PP substrates were converted to superhydrophobics after the treatments.

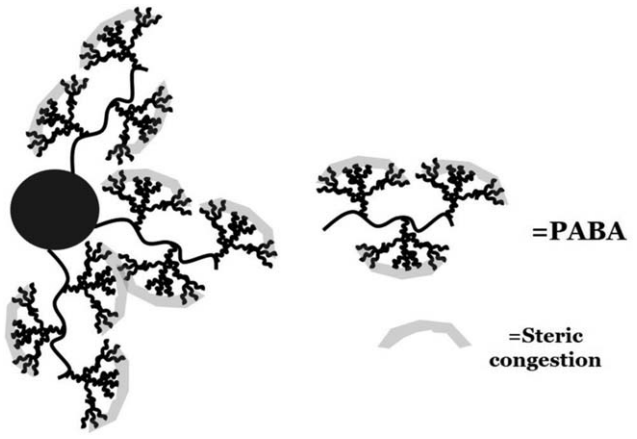

FIGURE 11 Schematization of steric congestion effects in NPs "core-brush" and NPs "core-dendrons."

The management of the organic silane concentration on the grafted TiO_2 NPs (NPs-CLE$^{5/90}$)-*g*-PABA and (NPs-CLE$^{10/90}$)-*g*-PABA allowed the self-cleaning properties of the PP surfaces to be controlled. When the organic silane/xylene ratio was 5/90 (v/v), larger craters were observed in the SEM images and a high CAH was measured (46 ± 5 degrees). In contrast, if a higher ratio of silane/xylene was used (10/90 v/v), the surfaces acquired self-cleaning properties with a CAH of 7.8 ± 0.7 degrees. Additionally, the WCA measured 162 ± 6 degrees was about 2.5% higher than the 5/90 ratio, and the SEM images showed more homogeneous surfaces with fewer craters. This probably decreased the liquid-solid contact area and consequently decreased the CAH. There are important antecedents of modified surfaces of other materials with superhydrophobic properties that showed WCA and CAH similar to those found by us in these hybrid surfaces. For example, steel sheet by the chemical etching and oxidation processes were obtained with WCA and CAH about 166 degrees and less than 2 degrees, respectively;[23] Cu surfaces grafted of poly(methyl methacrylate) (PMMA) showed WCA of 165.2 degrees;[22] superhydrophobic Ni-Cu-TiO_2 nanocomposite surfaces on the copper substrate was developed by electrodeposited coatings by myristic acid-ethanol solution with WCA of 161 degrees and the lowest CAH of 3 degrees.[16] In our previous published work,[25] superhydrophobic nanocomposite coatings on injection-molded polypropylene (PP) samples were prepared by dipping in xylene solvent containing different concentrations of titanium dioxide nanoparticles (NPs) functionalized with trimethoxypropyl silane. These materials showed a WCA between 150 and 160 degrees and CAH 23 and 1.5 degrees.

The TGA data showed that the weight loss in the temperature range between 100 and 500 °C was 15.63% and 21.68% for (NPs-CLE$^{5/95}$)-*g*-PABA and (NPs-CLE$^{10/90}$)-*g*-PABA, respectively, and this result was associated with the organic loading achieved at each synthetic step. This implies that there was a higher presence of hydrophobic and bulky functional groups, such as the *tert*-butyls as peripherical groups of dendritic monomers in the (NPs-CLE$^{10/90}$)-*g*-PABA. A higher presence of hydrophobic termination allowed superhydrophobic and self-cleaning PP surfaces to be obtained. The transition from the Wenzel to the Cassie Baxter regime may be controlled by the original organic silane/xylene ratio.

We can hypothesize that steric congestion is a consequence of the dendronization process, which may be justified by the "*umbrella*" protection effect exerted by the dendronized polymer chains grafted on the nanoparticles, as displayed in Figure 11. It is known that "core-brush" NP steric congestion occurs near the surface of NPs. In contrast, we postulate that in the case of dendronized NPs, steric congestion takes place away from these NPs (specifically at the periphery of the dendron screens), which thereby protects the surface of the NPs. In addition, another important property, as a consequence of the dendronization process, is that a high concentration of polymers grafted to NPs is not required to obtain superhydrophobic properties.

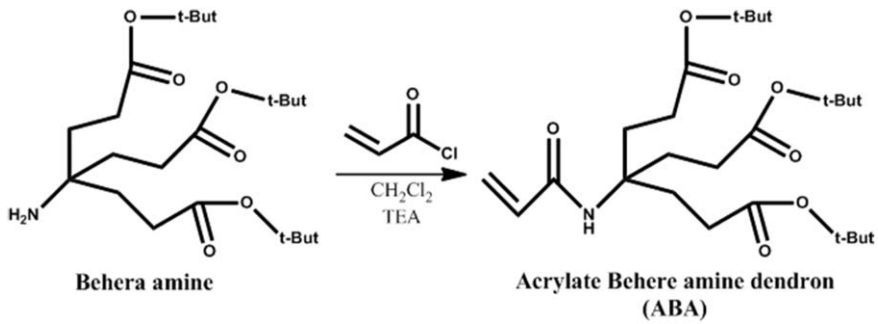

SCHEME 3 Synthesis of the dendritic monomer (ABA) obtained from Behere's amine and acryloyl chloride.

CONCLUSIONS

In conclusion, we have reported a novel synthesis and detailed characterization of polypropylene (PP) surfaces using hybrid nanomateriales from dendronized TiO_2 NPs, which demonstrated that they have superhydrophobic properties. The core-brush TiO_2 NPs were used as a building block for coating PP substrates. In agreement with previous publications we have demonstrated and highlighted the efficiency of the dendronization process as a tool in the use for surface functionalization in the search for new specific properties.

In particular, there are no antecedents concerning nanoparticles modified by SI-ATRP utilizing dendritic monomers, as explored in the present study.

EXPERIMENTAL

Materials

The titanium dioxide nanoparticle powder (AEROXIDE® TiO_2-P25) was obtained from Degussa Corporation, and amine Behera was from Frontier Scientific. The (3-chloropropyl) triethoxysilane (CLE), (3-chloropropyl) trimethoxysilane (CLM), hexamethyl triethylenetetramine (HMTETA), and xylene were obtained from Sigma Aldrich. Acryloyl chloride was synthetized by a procedure described by Stempel G.H et al. (Stempel, Cross and Mariella, 1950). Dichloromethane, ethanol, xylene, $NaHCO_3$ and $MgSO_4$ were purchased from Anedra. Polypropylene (PP) samples (Braskem S/A, 3.5 g/10 min) were injection-molded, washed ultrasonically with acetone for 30 min, dried at room temperature and then stored in a desiccator. The final PP substrates measured about 30×10 mm $\times$ 3 mm (thickness).

Preparation of Dendritic Monomer

The dendritic monomer [Acryl Behera's Amine (ABA)] was prepared according to a procedure described by Cuggino et al.[44] Briefly, acryloyl chloride (1.2 mL, 14.43 mmol) in dichloromethane (22 mL) was added dropwise over a period of 5 min (Scheme 3) to a stirred solution of Behera's amine (5.0 g, 12.03 mmol) and triethyl amine, TEA (3.4 mL, 24.06 mmol) in dichloromethane (110 mL) at 0 °C. Afterwards, stirring was maintained for 4 h at 25 °C.

After the reaction, ABA was purified by washing with $NaHCO_3$ solution in water. Next the organic phase was placed with anhydrous $MgSO_3$, filtered, and dried in a vacuum.

ABA was obtained with a 92% yield. ^{1}H-NMR (NMR symbol of Nuclear Magnetic Resonance) [δ (ppm): 1.47 (27 H, s); 2.06 (6 H, t, J = 7.5 Hz); 2.28 (6 H, t, J = 7.5 Hz); 5.62 (1 H, dd, J = 12, 1.5 Hz); 6.05 (1 H, dd, J = 19.0, 10.0 Hz); 6.24 (1 H, dd, J = 18.0, 1.5 Hz); 6.26 (1 H, s)]. ^{13}C-NMR [δ (ppm): 28.0; 29.8; 30.1; 57.6; 80.7; 125.8; 131.7; 164.8; 173.0]. FTIR (cm^{-1}): 3312 (N—H, amide), 3089 (C—H, vinyl), 1727 (C═O, ester), 1658 (C═O, amide), 1626 (C═C, vinyl).

Silanization of TiO_2 Nanoparticles

The functionalization process of NPs was performed by silanization using two different organic silane agents: (3-chloropropyl) triethoxysilane (CLE) and (3-chloropropyl) trimethoxysilane (CLM). CLE and CLM solutions of several concentrations were prepared in xylene at room temperature. Then, 50 mg of TiO_2 NPs were added to the prepared solutions and were sonicated for 3 h. Afterwards, the modified NPs were washed and recovered by dispersion-centrifugation cycles in ethanol to eliminate the non-attached organic silanes. In order to study the influence of the initiator in the polymerization on the NPs, different concentrations of organic silane/xylene were used (1/99, 5/95 y 10/90 v/v). The following products were obtained: NPs-CLE series: NPs-CLE$^{1/99}$, NPs-CLE$^{5/95}$, and NPs-CLE$^{10/90}$; NPs-CLM series: NPs-CLM$^{1/99}$, NPs-CLM$^{5/95}$, and NPs-CLM$^{10/90}$. The nomenclature CLE or CLM indicates the organic silane agent used, and the superscript identifies the organic silane/xylene ratio utilized in the prepared solutions.

ABA Grafting on Silanizated Nanoparticles

Grafting of the dendronized polymer was performed via SI-ATRP on previously functionalized NPs (NPs-CLE and NPs-CLM series). The NPs (50 mg) were dispersed in xylene (10 mL) in a two-neck flask equipped with a nitrogen inlet. Then, the ligand HMTETA and the ABA monomer were added in excess (6×10^{-5} mol/mg NPs). Three freeze-pump-thaw cycles were performed in order to create a vacuum in the system. Finally, a catalyst system (CuCl, $CuCl_2$) was added under N_2, with both the ligand and the catalyst system being at the same proportions as the NPs. The reaction was carried out at 40 °C for 48 h (polymerization was

stopped by opening the flask to permit air to enter). Finally, the modified NPs were washed and recovered by dispersion-centrifugation cycles in dichloromethane to eliminate the non-attached monomer. Type core-brush NPs of TiO_2 were obtained with brushes of poly(ABA) (PABA). The same procedure was performed on functionalized NPs surfaces without the ABA monomer

Preparation of Superhydrophobic Surfaces

To construct the superhydrophobic PP surfaces, the (NPs-CLE)-*g*-PABA series were selected. These surfaces were prepared following the dip-coating procedure previously reported.[25] Briefly, (NPs-CLE)-*g*-PABA were dispersed in xylene at 125 °C, and a PP stick was immersed for 3 sec, after which, the stick was dried in an oven at 100 °C.

Equipment and Characterization Techniques

Infrared Spectroscopy

Diffuse reflection Fourier transform (DRIFT) infrared spectra were recorded using a Nicolet 360 spectrometer (32 scans on average), at a resolution of 4 cm^{-1}. Infrared data were processed using Omnic 8.0 software.

ATR-FTIR

Attenuated Total Reflectance Fourier Transform Infrared (ATR-FTIR) interferograms were acquired using the same spectrometer equipped with an Attenuated Total Reflectance accessory, and a 45 ZnSe crystal (beam penetration is 1.67 μm) was used to monitor samples. All spectra were obtained for 32 scans on average, at a 4.0 cm^{-1} resolution in a range between 650 and 4000 cm^{-1}. Infrared data were processed using Omnic 8.0 software.

UV–Visible Spectrophotometry

UV spectra were recorded using a Shimadzu 1800 240 v spectrometer, at between 200 and 900 nm wavelengths at room temperature.

Transmission Electron Microscopy

TEM images were recorded using a JEOL 1200 EXII electronic microscope operating at 80 kV. Samples were prepared by dropcasting, where the dried NPs [(NPs-CLE)-*g*-PABA] were dispersed in ethanol. Then, drops of this dispersion were placed onto standard carbon-coated colodion film copper grids (200-mesh), which was followed by solvent evaporation. For each sample, a minimum of four different regions were studied. The estimated size of the NPs was calculated using the Image J public domain processing program. For the size determination of the bare TiO_2-NPs, (NPs-$CLE^{5/95}$)-g-PABA, and (NPs-$CLE^{10/90}$)-g-PABA were used 5, 4, and 4 TEM images, respectively.

Thermogravimetric Analysis

TGA data were obtained from DTG 60 Shimadzu equipment, under nitrogen flux (50 mL/min), in sealed aluminum pans heated up to 600 °C (10 °C/min).

The percentage of modification (p) of TiO_2 NPs by PABA, was calculated using TGA data according eq 1.[48]

Small-Angle X-Ray Scattering

SAXS experiments were performed using a Xeuss apparatus. The NPs [(NPs-CLE)-*g*-PABA] were dispersed in ethanol, and the measurement conditions were: sample-detector distance: 537 mm, q (min) = 0.18 nm^{-1}, beam size in the sample 0.5 mm^2, and room temperature (22 ° C).

Scanning Electron Microscopy

SEM images were recorded with an EVO 50 ZEISS and FE-SEM Σigma microscopes using electron acceleration between 3 and 5 kV. Samples were metallized with gold.

Profilometer Measurements

Profilometer measurements were carried out by using the optical profilometer Bruker Contour GTK. The arithmetic mean of the surface roughness (Ra) was calculated from the roughness profile and the root mean squared (RMS) roughness was obtained. For each sample three different modified sticks were studied, with all of these measurements being repeated at least five times for different positions.

Water Contact Angle Measurements

The static water contact angle (WCA) and contact angle hysteresis (CAH) were measured at ambient temperature using a drop of deionized water (4 μL), which was gently placed on the substrate using a micro syringe.

Contact Angle Hysteresis (CAH)

The advancing and receding contact angles were measured at the front and back of droplets, respectively, just before they moved along the tilted surface. Images were captured using a digital video camera (Surftens 3.0 software), with equipment specially designed for this purpose, and analyzed for contact angle measurements using Image J software. For each sample, three different modified sticks were studied, with all the measurements being repeated at least five times at different positions.

Adhesion Test

A 3M® tape was placed in contact with the PP stick and then removed after of 3 sec. Images of the stick surface (before and after the test) and an image of the tape were captured using an optical microscope in order to observe the amount of coating removed by the 3M® tape.

ACKNOWLEDGMENTS

The authors thank SECyT (Universidad Nacional de Cordoba, Res. 366/16), FONCyT (PICT-2015-2477), CONICET (PIP No. 112-20110101029), CNPq (Conselho Nacional de Desenvolvimento Científico e Tecnológico, Brazil), and Argentina-Brasil CAPES for financial assistance. C.B.C. also acknowledges receipt of fellowships from SECyT-UNC (2011–2013) and CONICET (2014–2015).

REFERENCES

1 Z. Yuan, Y. Shu, Y. Xin, B. Ma, *Chem. Commun.* **2016**, *52*, 3887.

2 T. Xiang, M. Zhang, C. Li, S. Zheng, S. Ding, J. Wang, C. Dong, L. Yang, *J. Alloys Compd.* **2017**, *704*, 170.

3 X. Yao, Y. Song, L. Jiang, *Adv. Mater.* **2011**, *23*, 719.

4 N. Valipour, F. C. Birjandi, J. Sargolzaei, *Colloids Surf. A Physicochem. Eng. Asp.* **2014**, *448*, 93.

5 P. Zhang, F. Y. Lv, *Energy.* **2015**, *82*, 1068.

6 G. Polizos, G. G. Jang, D. B. Smith, F. A. List, M. G. Lassiter, J. Park, P. G. Datskos, *Sol. Energy Mater. Sol. Cells.* **2018**, *176*, 405.

7 H. Zhou, Y. Zhao, H. Wang, T. Lin, *Adv. Mater. Interfaces.* **2016**, *3*, 1600402.

8 Z. Cui, L. Yin, Q. Wang, J. Ding, Q. Chen, *J. Colloid Interface Sci.* **2009**, *337*, 531.

9 M. Liu, S. Wang, Z. Wei, Y. Song, L. Jiang, *Adv. Mater.* **2009**, *21*, 665.

10 K. Liu, Y. Tian, L. Jiang, *Prog. Mater. Sci.* **2013**, *58*, 503.

11 Y. Liu, Q. Wang, X. Zhu, F. Yang, M. Y. Akram, J. Nie, *Mater. Lett.* **2017**, *190*, 48.

12 E. Jiaqiang, Y. Jin, Y. Deng, W. Zuo, X. Zhao, D. Han, Q. Peng, Z. Zhang, *Adv. Mater. Interfaces.* **2018**, *5*, 1701052.

13 Z. Yoshimitsu, A. Nakajima, T. Watanabe, K. Hashimoto, *Langmuir* **2002**, *18*, 5818.

14 C.-T. Hsieh, J.-M. Chen, R.-R. Kuo, T.-S. Lin, C.-F. Wu, *Appl. Surf. Sci.* **2005**, *240*, 318.

15 B. Bhushan, M. Nosonovsky, Y. C. Jung, *J. R. Soc. Interface.* **2007**, *4*, 643.

16 H. Bagheri, M. Aliofkhazraei, H. M. Forooshani, A. S. Rouhaghdam, *Appl. Surf. Sci.* **2018**, *436*, 1134.

17 R. N. Wenzel, *J. Ind. Eng. Chem.* **1936**, *28*, 988.

18 A. B. D. Cassie, S. Baxter, *Trans. Faraday Soc.* **1944**, *40*, 546.

19 H. Zhao, K.-Y. Law, V. Sambhy, *Langmuir.* **2011**, *27*, 5927.

20 M. E. Kavousanakis, C. E. Colosqui, I. G. Kevrekidis, A. G. Papathanasiou, *Soft Matter* **2012**, *8*, 7928.

21 E. S. Savoy, F. A. Escobedo, *Langmuir* **2012**, *28*, 3412.

22 J. Cai, S. Wang, J. Zhang, Y. Liu, T. Hang, H. Ling, M. Li, *Appl. Surf. Sci.* **2018**, *436*, 950.

23 Y. Liu, W. Yao, X. Yin, H. Wang, Z. Han, L. Ren, *Adv. Mater. Interfaces.* **2016**, *3*, 1500723.

24 Y. Y. Yan, N. Gao, W. Barthlott, *Adv. Colloid Interface Sci.* **2011**, *169*, 80.

25 C. B. Contreras, G. Chagas, M. C. Strumia, D. E. Weibel, *Appl. Surf. Sci.* **2014**, *307*, 234.

26 A. T. Abdulhussein, G. K. Kannarpady, A. B. Wright, A. Ghosh, A. S. Biris, *Appl. Surf. Sci.* **2016**, *384*, 311.

27 G. K. Belmonte, G. Charles, M. C. Strumia, D. E. Weibel, *Appl. Surf. Sci.* **2016**, *382*, 93.

28 H. Li, S. Yu, *Appl. Surf. Sci.* **2017**, *420*, 336.

29 A. A. Motedayen, C. Guillaume, E. Gastaldi, O. Félix, N. Gontard, *RSC Adv.* **2016**, *6*, 75640.

30 T. Kim, J.-H. Kim, T. E. Kang, C. Lee, H. Kang, M. Shin, C. Wang, B. Ma, U. Jeong, T.-S. Kim, B. J. Kim, *Nat. Commun.* **2015**, *6*, 8547.

31 Z. Yuan, Y. Shu, Y. Tian, Y. Xin, B. Ma, *Chem. Commun.* **2015**, *51*, 16385.

32 C. Zhou, Y. Tian, Z. Yuan, M. Han, J. Wang, L. Zhu, M. S. Tameh, C. Huang, B. Ma, *Angew. Chemie Int. Ed.* **2015**, *54*, 9421.

33 S. G. R. Bade, J. Li, X. Shan, Y. Ling, Y. Tian, T. Dilbeck, T. Besara, T. Geske, H. Gao, B. Ma, K. Hanson, T. Siegrist, C. Xu, Z. Yu, *ACS Nano.* **2016**, *10*, 1795.

34 J. I. Paez, M. Martinelli, V. Brunetti, M. C. Strumia, *Polymers (Basel).* **2012**, *4*, 355.

35 H. Frauenrath, *Prog. Polym. Sci.* **2005**, *30*, 325.

36 S. D. Garcia Schejtman, V. Brunetti, M. Martinelli, M. C. Strumia, In *Hybrid Polymer Composite Materials*, Elsevier: New York, **2017**.

37 A. A. Aldana, M. C. Strumia, M. Martinelli, *Aust. J. Chem.* **2015**, *68*, 1918.

38 G. N. Rimondino, E. Miceli, M. Molina, S. Wedepohl, S. Thierbach, E. Rühl, M. Strumia, M. Martinelli, M. Calderón, *J. Mater. Chem. B* **2017**, *5*, 866.

39 E. Mohammadifar, A. Nemati Kharat, M. Adeli, *J. Mater. Chem. B* **2015**, *3*, 3896.

40 A. A. Aldana, R. Toselli, M. C. Strumia, M. Martinelli, *J. Mater. Chem.* **2012**, *22*, 22670.

41 J. I. Paez, E. A. Coronado, M. C. Strumia, *J. Colloid Interface Sci.* **2012**, *384*, 10.

42 E. D. Farías, J. I. Paez, M. C. Strumia, A. M. Baruzzi, M. C. G. Passeggi, V. Brunetti, *Electrochim. Acta.* **2014**, *134*, 76.

43 S. D. García Schejtman, R. Toselli, M. C. Strumia, M. Martinelli, *Polym. Bull.* **2015**, *72*, 3043.

44 J. C. Cuggino, M. Calderón, C. I. Alvarez, M. C. Strumia, K. N. Silva, E. K. Penott-Chang, A. J. Müller, *J. Colloid Interface Sci.* **2011**, *357*, 147.

45 J. T. Park, J. H. Koh, J. K. Koh, J. H. Kim, *Appl. Surf. Sci.* **2009**, *255*, 3739.

46 H. Esen, *Des. Monomers Polym.* **2015**, *18*, 745.

47 A. Craievich, In *Handbook of Sol-Gel Science and Technology*, Kluwer Academic Publishers: New York, **2005**.

48 V. G. Ngo, C. Bressy, C. Leroux, A. Margaillan, *Polymer (Guildf).* **2009**, *50*, 3095.